AD-A052 576 MISSION RESEARCH CORP SANTA BARBARA CALIF F/G 17/2.1
AN AMBIENT HE RADIO MODE MODEL.(U)
SEP 77 D H SOWLE DNA001-76-C-0349
UNCLASSIFIED MRC-R-347 DNA-4420T NL

1 OF 1
ADA
052 576

END
DATE
FILMED
5-78
DDC

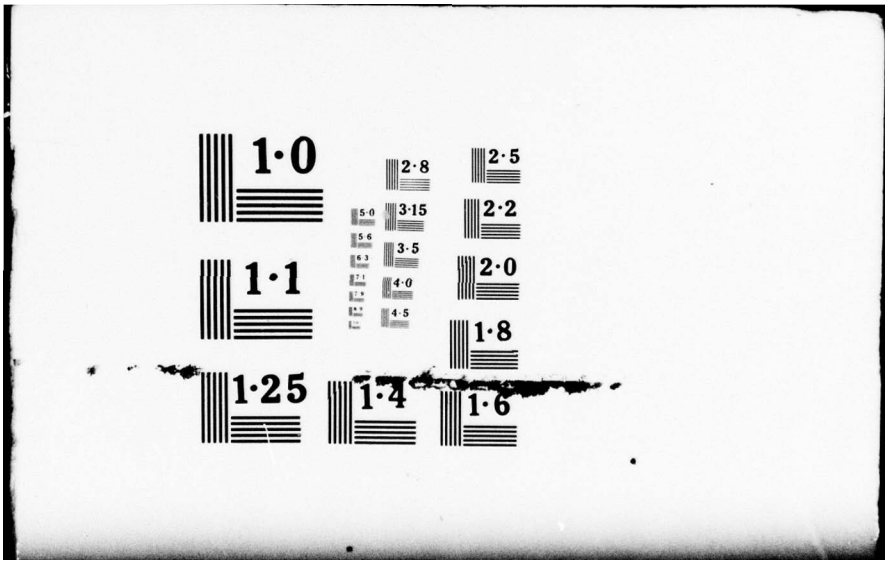
1·0
1·1
1·25
1·4
1·6
1·8
2·0
2·2
2·5
2·8
3·15
3·5
4·0
4·5
5·0
5·6
6·3

DNA 4420T

AN AMBIENT HF RADIO MODE MODEL

Mission Research Corporation
735 State Street
Santa Barbara, California 93101

September 1977

Topical Report for Period February 1977—September 1977

CONTRACT No. DNA 001-76-C-0349

THIS WORK SPONSORED BY THE DEFENSE NUCLEAR AGENCY
UNDER RDT&E RMSS CODE B32207T464 S99QAXHB05305 H2590D.

Prepared for
Director
DEFENSE NUCLEAR AGENCY
Washington, D. C. 20305

Destroy this report when it is no longer needed. Do not return to sender.

(18) DNA, SBIE (19) 4420T, AD-E300 154 (12) 50p.

UNCLASSIFIED
SECURITY CLASSIFICATION OF THIS PAGE (When Data Entered)

REPORT DOCUMENTATION PAGE

READ INSTRUCTIONS BEFORE COMPLETING FORM

1. REPORT NUMBER: DNA 4420T
2. GOVT ACCESSION NO.
3. RECIPIENT'S CATALOG NUMBER

4. TITLE (and Subtitle): (6) AN AMBIENT HF RADIO MODE MODEL.

5. TYPE OF REPORT & PERIOD COVERED: (9) Topical Report for Period Feb 77—Sep 77

6. PERFORMING ORG. REPORT NUMBER: (14) MRC-R-347

7. AUTHOR(s): (10) D. H. Sowle

8. CONTRACT OR GRANT NUMBER(s): (15) DNA 001-76-C-0349

9. PERFORMING ORGANIZATION NAME AND ADDRESS:
Mission Research Corporation
735 State Street
Santa Barbara, California 93101

10. PROGRAM ELEMENT, PROJECT, TASK AREA & WORK UNIT NUMBERS: (16) NWED Subtask S99QAXHB053-05 (17) BD53

11. CONTROLLING OFFICE NAME AND ADDRESS:
Director
Defense Nuclear Agency
Washington, D.C. 20305

12. REPORT DATE: (11) Sep 77

13. NUMBER OF PAGES: 56

14. MONITORING AGENCY NAME & ADDRESS (if different from Controlling Office)

15. SECURITY CLASS (of this report): UNCLASSIFIED

15a. DECLASSIFICATION/DOWNGRADING SCHEDULE

16. DISTRIBUTION STATEMENT (of this Report)

Approved for public release; distribution unlimited.

17. DISTRIBUTION STATEMENT (of the abstract entered in Block 20, if different from Report)

18. SUPPLEMENTARY NOTES

This work sponsored by the Defense Nuclear Agency under RDT&E RMSS Code B32207T464 S99QAXHB05305 H2590D.

19. KEY WORDS (Continue on reverse side if necessary and identify by block number)

High Frequency
Mode Calculation

20. ABSTRACT (Continue on reverse side if necessary and identify by block number)

An approximate method for calculation of high frequency skywave radio propagation geometry is developed. The method is inexpensive in comparison to ray trace techniques yet capable of accounting for instantaneous local ionospheric conditions including tilt and off-great-circle propagation. It is thus appropriate for use in assessment of system response to nuclear effects on HF propagation, including alterations of mode geometry. Errors inherent in the approximations are shown to be small compared to errors caused by inaccuracies in ambient or disturbed ionospheric models.

DD FORM 1 JAN 73 1473 EDITION OF 1 NOV 65 IS OBSOLETE

UNCLASSIFIED
SECURITY CLASSIFICATION OF THIS PAGE (When Data Entered)

406548

CONTENTS

1. INTRODUCTION

A model of high frequency radio (HF) skywave modes under ambient conditions is basic to the study of HF system response to disturbed conditions, such as those which would be encountered in a nuclear conflict.

Traditionally, HF skywave vulnerability has been calculated under the assumptions that only D-layer absorption is important, that ambient propagating modes are an adequate approximation to modes which propagate after nuclear explosions, and that a careful description of late time (ten minutes to hours) debris motion is unnecessary so long as an assured defense conservative model is used.

Recent interest in adaptive HF systems for the Air Force and MEECN, as well as interest in the closely related class of meteor burst communication systems, has forced a re-evaluation of all three of the above assumptions. More realistic models of late time nuclear debris motion (the source of nuclear radiations which ultimately cause D-layer absorption) have recently been developed[1,2] to allow improved absorption calculations. In this report we describe a method of ambient HF skywave mode calculation designed to readily accept disturbed ionospheric conditions, and thus to allow inclusion of some nuclear disturbances important to propagation geometry, necessary for more accurate calculation of D-layer absorption effects as well as for removal of the second and third traditional assumptions quoted above.

The necessity for development of an ambient skywave propagation mode calculation requires justification. Elaborate techniques for detailed calculation exist in the scientific community,[3] which have been adapted into a nuclear effects code.[4] Less elaborate techniques exist for long term average mode prediction,[5] to which simplified fits have been made, and these fits are commonly used in the nuclear effects community.[6] To understand the requirement for a technique of intermediate complexity requires a brief discussion of anticipated nuclear effects of HF propagation in relation to characteristics of available calculational techniques.

Anticipated nuclear effects which may conveniently be taken into account by alteration of normal ionospheric parameters are changes in ambient layer (i.e., F2, F1, or E-layer) electron density, thickness, height, and tilt due to: (1) propagating acoustic gravity waves, (2) ducted waves, (3) burst region disturbance (F-layer depletion, etc.), or (4) bomb or debris irradiation. Another set of effects exists (M-modes, fireball modes, plume modes, etc.) which are more conveniently calculated independently and which will not concern us here. To calculate, even crudely, effects of the above list on propagation geometry, thus on existence and efficacy of ambient-like modes and creation of new modes, the ambient mode calculation must readily take into account ionospheric variations all along the propagation path in terms of variability of reflection height and ionospheric tilt, both along and across the great circle path. In fact, non great circle propagation must be treated. The current ITS78 code,[5] the community standard, evaluates ionospheric conditions only at the great circle path center, derives from that a single reflection height, and does not consider tilt or off-great circle propagation. This is satisfactory for long term average predictions, the objective of that code, but does not lend itself to situations similar to nuclear effects where a portion of the path is strongly disturbed. The WRECS code,[6] using a fit to ITS78 predictions, allows for two values of reflection height corresponding to

day or night but is otherwise restricted to ITS78 predictions. The NUCOM code[4] uses ray tracing techniques and thus can be much more versatile, but such techniques are expensive for our purposes.

The method developed here to meet requirements of nuclear effects studies is approximate but more accurate than justified by predictability of either the ambient or nuclear disturbed ionosphere. It is more expensive in computer time than one would prefer but still vastly cheaper than normal ray trace techniques; sophisticated in that it accounts for ionospheric variation, tilt, and off-great circle propagation; but in its present implementation rudimentary in that only two modes can be calculated for a given number of hops, no extraordinary ray modes are calculated, etc. The restriction to two modes per hop number could be readily remedied and this, at least, is hoped to be done soon. The basic technique is believed to be sufficiently versatile that extension toward more realistic treatment is feasible. As reported here the method has been develoepd to a useful state, one that is more realistic than others in many important respects, as well as one that is reasonably inexpensive in application.

An outline of the overall calculation is given in the next section and specific components discussed in following sections.

2. OUTLINE OF THE CALCULATION

The calculation is naturally broken into two logical modules, each of which consists of several component subroutines.

2.1 Ionospheric Data

The first module is exercised once only, before any propagation calculations are attempted. It uses an ionospheric model to create a data table of ionospheric parameters for each desired transmitter-receiver link. Each such data table consists of three sets (one for each ionospheric layer, E, F1, F2) of three parameters describing parabolic ionospheric layers above several points on the great circle path at a number of times. The three layer parameters are: (1) maximum electron density, (2) thickness of the layer, and (3) altitude of the maximum electron density. The spatial points are arbitrary in number and spaced equally along the great circle path. The number of times is also arbitrary and determines a number of equal segments of a twenty-four hour period at which each layer will be specified at each point along the great circle. Normally we choose twenty-four times, one for each hour of the day (plus one repeated entry to allow the table to begin at 0 hours and end at 24 hours), and seven space points; which yield six equally spaced points along the path (both end points are included), normally these great circle points are separated by less than 15° of arc each (that is, corresponding to less than an hour apart local time). With ionospheric models at our disposal[5,7] one hour equivalent segments have been found to be about twice as dense as necessary to allow interpolation in both space and time to the limit of model fidelity.

The purpose of this array of (3 layers) × (3 parameters) × (typically 7 space points) × (typically 25 time points) = 1575 numbers per link is to allow rapid interpolation in space and time for ionospheric

quantities without having to repeatedly calculate potentially complex ionospheric models for identical or similar conditions. Heights and thicknesses are interpolated linearly between adjacent points and electron density logarithmically. In Section 5 we shall show that despite appearances, this form of ionospheric data table does not restrict consideration to great circle paths.

A typical comparison of the three parabolic layer ionospheric approximation used here to the ITS78 model,[5] the Aerospace Model[7] and to data[7] is shown in Figure 1. Cases can be found in which the three-layer approximation fits the model somewhat better and somewhat worse than Figure 1. It is also easy to find both better and worse comparisons between the models and data. Figure 1 illustrates the general result, which appears to be valid for all ionosphere models which might be used as a basis for the fit, that error resulting from the three parabolic layer approximation is small compared to error due to the uncertain behavior of the real ionosphere.

2.2 Mode Calculation

The second module calculates mode geometry. Inputs to this module are a specified time, ray type, link, frequency, and number of hops. All of these quantities are arbitrary except for obvious restrictions, frequency and number of hops must be greater than zero; and except for a bow to the nature of Fortran compilers, presently we dimension for no more than eight hops. The ray type specifies either the low ray or high (Pederson) ray. Outputs of this module are either specification of mode geometry or information concerning the reason no such mode exists.

Mode geometry is specified in terms of the ends of a number of straight line segments (passes) connecting reflection points. A one-hop mode is specified by latitude, longitude, and altitude above the earth's surface of three line segment ends; (1) the transmitter coordinates,

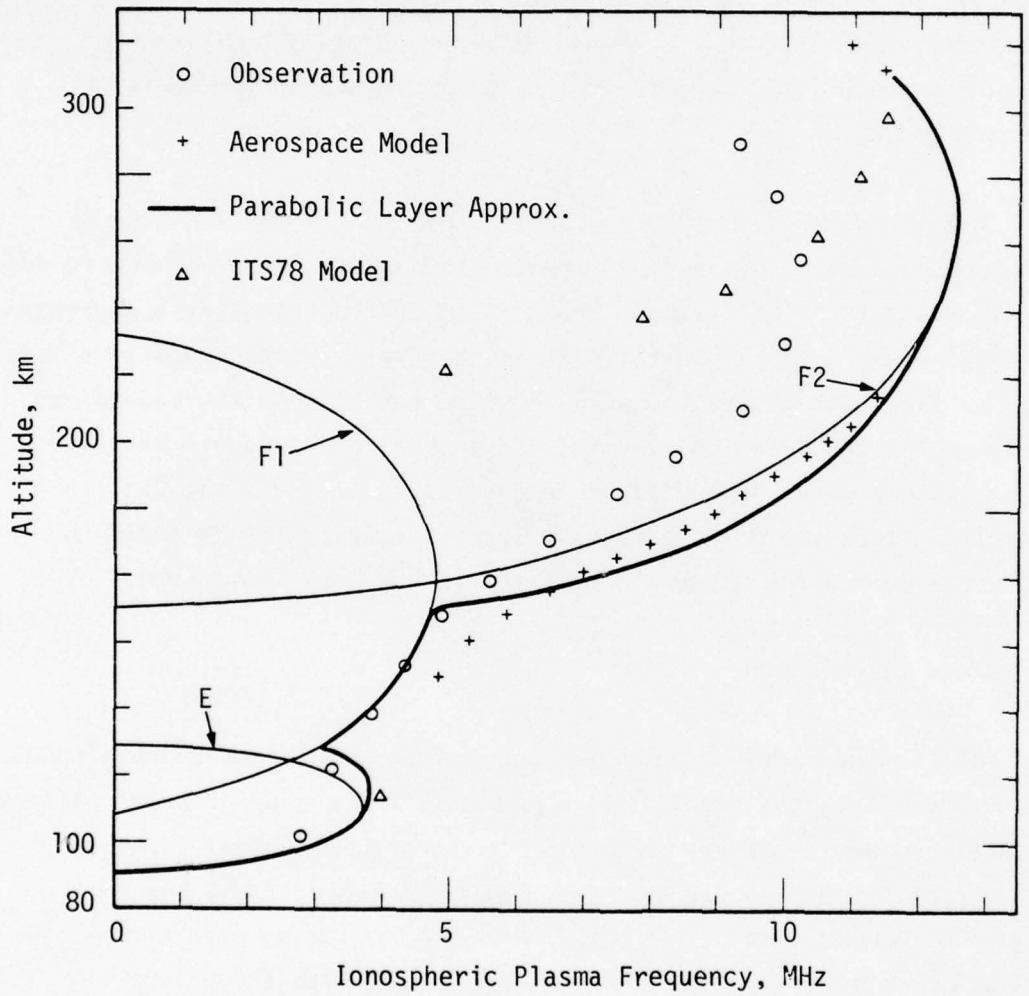

Figure 1. Typical ambient ionosphere. The HFNET three parabolic layer fit is compared to the Aerospace model from which it is derived, to the ITS78 model, and to data for 1200 local time above Arecibo, Puerto Rico, Dec. 1968. Smoothed Zurich sunspot number is 110.

(2) the equivalent triangular ionospheric reflection point, and (3) the receiver coordinates. A two-hop mode requires specification of coordinates for five points; the two end points, two ionospheric reflection points, and an intermediate surface reflection point. In general three-space coordinates must be specified for 2n + 1 points for an n-hop mode.

A mode fails to exist if: (1) the F2 layer fails to reflect the ray on any hop, (2) transmitted launch angle for the mode is below a specified value, (3) received angle is below a specified value, (4) ionospheric tilt causes the ray to be reflected back upon itself, or (5) ionospheric tilt causes the ray to be deflected forward at too great an angle.

Steps in calculation of n-hop mode geometry are as follows:

1. The great circle path is divided into n equal segments, one for each hop.
2. For each segment a one-hop mode is calculated according to local ionospheric conditions as follows:
    a. Assume reflection occurs at the F2-layer; calculate the equivalent triangular reflection altitude, h_r, for a parabolic layer by iteration patterned after Reference 5.
    b. If successful, calculate refraction effect due to the F1 layer. If the F1 layer reflects the ray, carry out (a) for the F1 layer.
    c. Calculate refraction effect due to the E-layer. If the E-layer reflects the ray, carry out (a) for the E-layer.

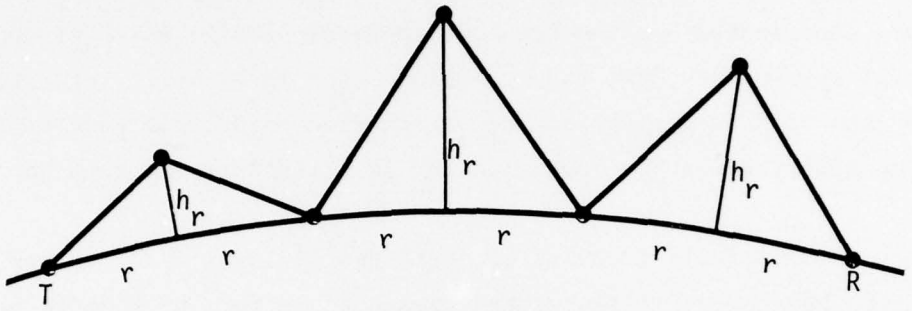

The situation at the end of step (2) is depicted in the sketch, provided all hops were successfully reflected. At this point in the calculation the mode is specified by latitude and longitude end points equally spaced along the great circle path but each ionospheric reflection height is different, a violation of the laws of optics.

3. Adjust the pass ranges, r_i, so that incident and reflected angles are equal, accounting for differences in h_r.

4. Calculate ionospheric tilt angles both along the great circle and across the great circle at each ionospheric reflection point.

5. Adjust all pass coordinates (latitude, longitude, altitude) to account for tilt along the great circle to first order in tilt angle (that is, in the vicinity of each reflection point, the tilt is constant). If the ray is reflected back upon itself at any point, or if the cumulative effect of all tilts cause the ray to land too far beyond the receiver, reject the mode.

6. Calculate off-great circle displacements of all pass coordinates and new reflection altitudes due to across great circle tilt.

7. Find launch and received ray elevation relative to the horizon, and azimuth relative to the great circle path. If either elevation is below a specified limit, reject the mode.

At the end of this process an approximation has been found to a "good" propagating mode with specified number of hops, within the limitations indicated above.

Possible paths which include hops of the form indicated in the sketch are not found. The situation depicted in (a) is rejected because

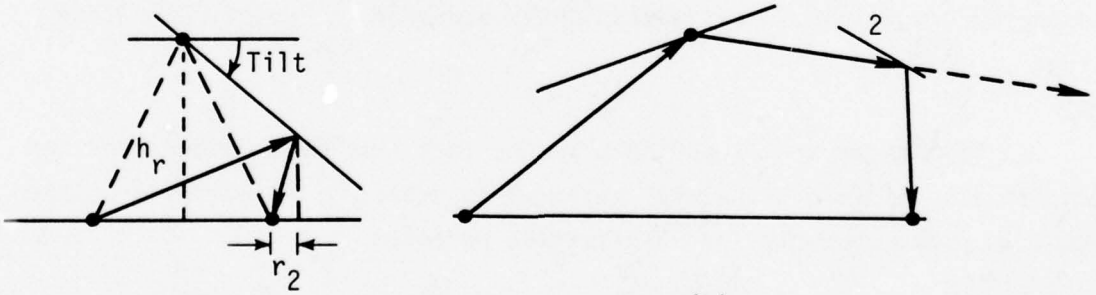

(a) (b)

r_2 is negative, the ray was reflected back upon itself. Within the mathematical restrictions of first order tilt angle treatment this situation can only arise when h_r is greater than the chord between the two ground points, and can only represent a reasonably plausible situation when the second point represents receiver or transmitter. These conditions are too severe for ambient skywave propagation. Situation (b) is rejected because the calculation

does not allow for existence of the second reflection point, 2, and assumes that the ray continues along the dotted path. This situation seems unlikely under ambient conditions but could occur in a disturbed environment. It must be handled, if at all, in future as a "disturbed" mode, with appropriate logic specified.

The reader will note that no step between (1) and (7) was iterated. The only iterations occur in finding single-hop solutions to reflection from a single parabolic layer in step (2). With this exception the mathematical treatment runs "open loop" and could be made more rigorous by iterating on each refraction correction, after range correction for differing reflection heights, and after corrections for tilt. Such a procedure would be prohibitively expensive in calculation time and would produce numerical results significantly different from the present technique only for cases where some reflection occurred very near a critical point (e.g., almost or barely reflected off some layer). Predictability of either natural or disturbed ionospheric conditions is not sufficiently accurate to justify such fine tuning.

Of much greater importance is the fact that this method does not calculate all possible "sensible" rays. This defect is illustrated in the sketch, in plane geometry for illustrative purposes.

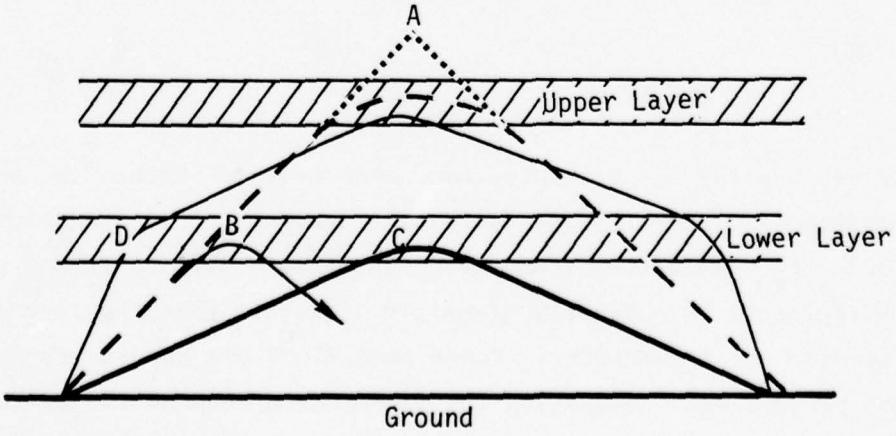

Our technique first finds a tentative (low or Pederson) ray which reflects off the highest available layer, the dashed ray of the sketch which reflects in the vicinity of point A. Next the refraction angle due to passage through the lower layer at point B is calculated. If refraction is not large enough to reflect the ray at B, a correction to the effective triangular reflection point A is introduced and calculation proceeds to the next step. At this point our technique has irretrievably missed a potential lower ray which reflects at C. Under almost all ambient conditions the lowest ray suffers greater absorption and also is a more likely candidate for rejection due to low launch angle, thus is not likely to be useful or to cause multipath problems. It is unusual but possible that nuclear effects could preferentially interfere with the upper ray enough to make the ray at C the best mode. This is a weakness in current logic which probably should be fixed.

On the other hand, if the ray is reflected at B then the technique shifts attention to the lower layer and calculates only the ray which reflects at C. Another option would be to search at higher angles for a ray which is strongly refracted at D, closer to the critical angle for the frequency if such exists, and which traverses the path indicated by the light solid line, a high ray.

Thus the technique will select preferentially the dashed ray, then the heavy ray; but not both.

The only time the method selects a ray like that refracting at D is in the rare instance when point B happens to lie very near the critical angle for the lower layer. This feature is generally good because when refraction occurs in the vicinity of the critical angle a significant defocusing occurs with attendant loss of signal strength. But if strong D-layer absorption occurs on the heavy ray, the defocusing loss at D could be less than absorption loss; in this event the method misses the best

propagating path. Again, a more elaborate procedure could be devised to cure this weakness.

Other cases of interest which are not handled at present include spread F and sporatic E multipath, and cases where unusual spatial dependence of the layers produce freak (but occasionally real) propagation paths.

In summary, the selected technique is believed to produce the strongest propagating mode under most conditions, but has weaknesses in that occasionally a potentially significant alternate mode is missed. The most important improvement would be to include sporatic E and spread F effects. These can be treated to an adequate approximation for many cases as a perturbation on the successful ray without incurring a significant penalty in computation time or logic. Treatment of other alternate rays will incur a noticeable penalty in computation time, and to some extent in complexity of logic.

3. SINGLE HOP CALCULATION

After the great circle path for an n-hop mode has been divided into n equal segments, each hop is calculated independently, as indicated in steps (1) and (2) of Section 2. Here we discuss step (2), calculation of a single reflection from a single parabolic layer, and correction for refraction in passage through a single parabolic layer.

3.1 Reflection

Our technique differs from that of Reference 5 substantially only in rearrangement of their iteration scheme. For more details the interested reader is referred to Reference 5.

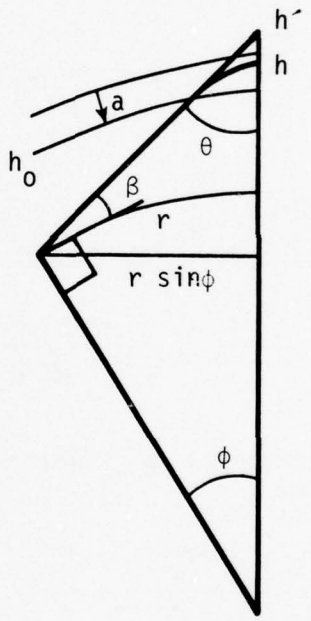

The scheme is a prediction-correction method based on the quantity

$$x = \alpha c \cos\theta \ , \qquad (1)$$

where α is the ratio of broadcast frequency to critical frequency at reflecting layer maximum, ω/ω_c. The factor c is a correction for ionospheric curvature, and θ is defined in the sketch.

Let h_o be altitude of the layer bottom and a be layer thickness, then the apparent reflection height ("equivalent" or "equivalent triangular" height), corresponding to an assumed value of x is

$$h' = h_o + \frac{ax}{2} \ln\left(\frac{1+x}{1-x}\right) \quad . \tag{2}$$

Now the tangent to the angle θ can be calculated from

$$\tan\theta = \frac{\sin\phi}{\frac{h'}{R_e} + (1-\cos\phi)} \tag{3}$$

where R_e is the earth's radius.

Also, the true maximum ray height can be calculated,

$$h = h_o + a\left(1 - \sqrt{1 - x^2}\right) \quad . \tag{4}$$

Next the curvature correction is calculated,

$$c = \sqrt{1 - \frac{2(h'-h)}{(R_e+h_o)} \tan^2\theta} \quad . \tag{5}$$

Finally, using the trigonometric identity,

$$\cos\theta = (1 + \tan^2\theta)^{-1/2} \quad , \tag{6}$$

the predicted values of x can be calculated (from (1)).

To start the iteration we calculate three values of x given initial guesses

$$x(x_1) \ , \quad x(x_2) \quad , \quad x(x_3) \quad .$$

Assuming the calculated value of x to be a quadratic function of the input value, we can solve for two values of input x which should reproduce themselves,

$$x_n = x_o \pm \sqrt{F_o/B}$$

where

$$x_o = \frac{1}{2}\,[x_1^2 - x_2^2 - R(x_3^2 - x_2^2)]/[(x_1 - x_2) - R(x_3 - x_2)]$$

$$R = [x(x_1) - x(x_2)]/[x(x_3) - x(x_2)]$$

$$B = [x(x_1) - x(x_2)]/[x_1^2 - x_2^2 - 2x_o(x_1 - x_2)]$$

$$F_o = x(x_1) - B(x_1 - x_o)^2 \qquad (7)$$

If $F_o > x_o$ then no solution exists, the ray penetrates the ionosphere.

It is necessary to place a logical guard against prediction of negative x; if this occurs set

$$x_n = x_{n-1}/2 \quad . \qquad (8)$$

It is also necessary to guard against prediction of $x_n > 1$, if this occurs set

$$x_n = (1 - x_{n-1})/2 \quad , \qquad (9)$$

We use $x_1 = 0.1$, $x_2 = 0.5$, $x_3 = 0.9$ and require for convergence

$$|x(x_n) - x_n| < 10^{-3} \quad .$$

So far, no case tried has required as many as ten iterations to converge.

3.2 Refraction by Passage Through a Lower Layer

This correction is also based upon Reference 5. We seek the change in launch angle, Δ, caused by the presence of a parabolic layer of thickness a_L whose maximum electron density occurs at altitude h_L. The previous solution for h' allows determination of the unperturbed launch angle, β. Then, from the sketch the crossing angle is given by

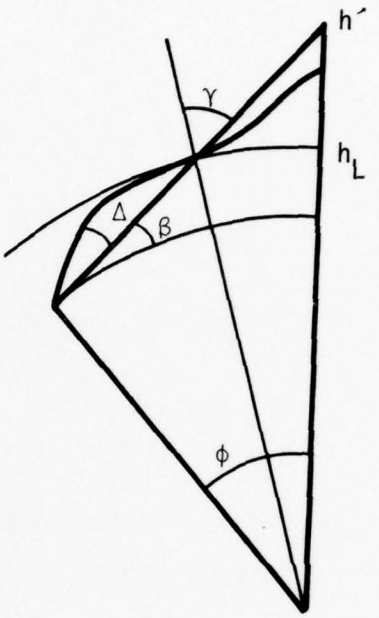

$$\sin\gamma = \cos\beta/(1+h_L/R_e) \quad . \tag{10}$$

Define

$$u \equiv \frac{\omega_L}{\omega\cos\gamma} \quad , \tag{11}$$

where ω_L is the maximum critical frequency of the refracting layer and ω is broadcast frequency.

If $u \geq 1$ the lower layer reflects the ray and one must recalculate h'.

If $u < 1$ then, from Reference 5

$$\Delta = 2\,\frac{a_L \tan\gamma}{(R + h_L)}\left[\frac{1}{2u}\,\ell n\left(\frac{1+u}{1-u}\right) - 1\right] \quad . \tag{12}$$

The corrected launch angle is

$$\beta' = \beta + \Delta \quad , \tag{13}$$

and h' can now be recalculated, including refraction effects.

This procedure is repeated for each layer below the reflecting layer.

4. RANGE ADJUSTMENT FOR DIFFERING REFLECTION HEIGHTS

The method chosen is sufficiently accurate for our purposes but is more cumbersome than one would prefer.

4.1 Method

For orientation we first work out the case of a flat earth.

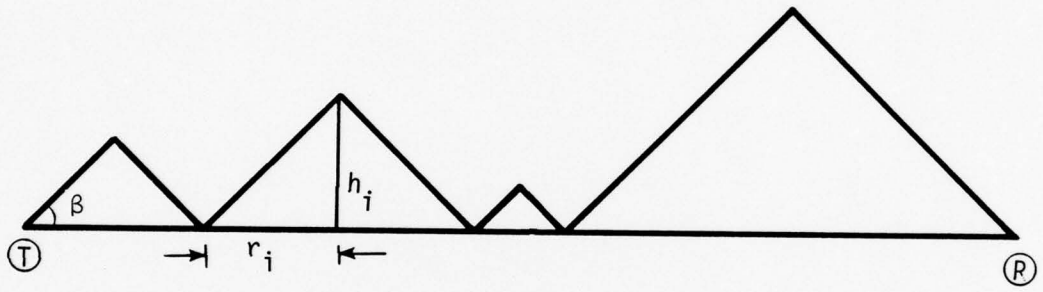

Given the number of hops and an arbitrary set of reflection altitudes, h_i, we seek the launch angle, β, and the set of pass ranges, r_i, which allow β to be constant at each reflection point.

We have

$$\tan\beta = h_i/r_i \tag{14}$$

Then

$$r_i = h_i/\tan\beta \tag{15}$$

and the total range, R, is

$$R = \frac{1}{\tan\beta} \sum_i h_i \tag{16}$$

So the launch angle can be found from

$$\tan\beta = R^{-1} \sum_i h_i \tag{17}$$

and individual pass ranges from (15).

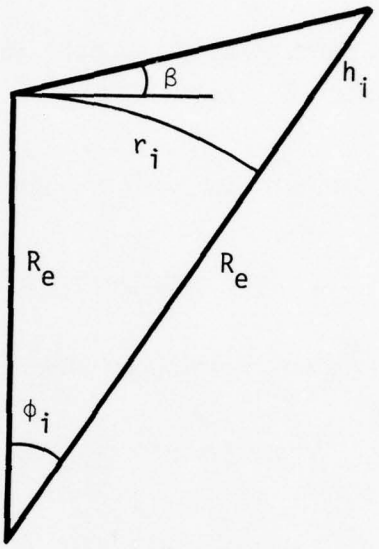

With the solution to this easy problem in mind, we now proceed to search for an approximate solution to the curved earth problem. In this case all of the surface reflection angles will again have a common value β, as illustrated in the sketch on p 20. Failing to find a neat closed form solution to the problem we proceed to find an approximation which resembles (14) and is accurate for $h_i/R_e << 1$. Such an approximation is

$$\tan\beta = \frac{h_i}{r_i} \frac{[1 - r_i^2/(2h_iR_e)]}{(1 + h_i/R_e)} \tag{18}$$

Equation 18 is good to about 10 percent for h_i of 3000 km and r_i small compared to R_e, and becomes better rapidly as h_i approaches realistic reflection altitudes of a few hundred kilometers.

Proceeding as in the plane case, we solve (18) for r_i

$$r_i = R_e \left[\sqrt{2x_i + (1+x_i)^2 \tan^2\beta} - (1+x_i)\tan\beta \right] . \tag{19}$$

where $x_i \equiv h_i/R_e$.

At this point it is clear that a problem exists, for if one sums Equation 19 to force agreement with the total range, analogous to the method by which (16) was obtained, we shall not be able to readily solve for $\tan\beta$.

Accordingly, we make further approximations by studying large β and small β limits.

If β is large enough (19) can be expanded to obtain

$$r_i = \frac{h_i}{(1+h_i/R_e)\tan\beta} + O(h_i^2) \quad . \tag{20}$$

Then, summing as before

$$\tan\beta = R^{-1} \sum_i \frac{h_i}{(1+h_i/R_e)} \quad , \tag{21}$$

which looks much like the plane case solution, Equation 17.

This large β limit occurs in practice but unfortunately will not be exclusive, or even common, in most situations. The small β limit is

$$r_i = \sqrt{2R_e h_i} - (R_e+h_i)\tan\beta + \frac{(R_e+h_i)^2 \tan^2\beta}{2\sqrt{2R_e h_i}} \quad . \tag{22}$$

Summing (22) to find total range and solving for $\tan\beta$ yields

$$\tan\beta = C/B - \sqrt{C^2/B^2 + 2(R-A)/B} \tag{23}$$

where

$$\left.\begin{aligned} A &\equiv \sum_i \sqrt{2\,R_e h_i} \\ B &\equiv \sum_i (R_e+h_i)^2/\sqrt{2R_e h_i} \\ C &\equiv \sum_i (R_e+h_i) \end{aligned}\right\} \tag{24}$$

Behavior of the two limiting solutions can be conveniently studied by choosing a case where all h_i are equal, then the large β limit, Equation 21, becomes

$$\tan\beta = \frac{Nh}{R(1+h/R_e)} \tag{25}$$

where N is twice the number of hops.

The small β limit, Equation 23 becomes

$$\tan\beta = \frac{\sqrt{2R_e h}}{(R_e+h)} \left[1 - \sqrt{\frac{2R}{N\sqrt{2R_e h}} - 1} \right] . \tag{26}$$

Define

$$\left.\begin{aligned} q &\equiv \sqrt{2N^2\, hR_e/R^2} \\ F &\equiv N(R_e+h)\,\tan\beta/R \quad , \end{aligned}\right\} \tag{27}$$

and

then Equation 25 becomes

$$F_L = q^2/2 \tag{28}$$

and Equation 26 becomes

$$F_s = q\ (1 - \sqrt{2/q-1}) \tag{29}$$

The behavior of F vs. q is illustrated in Figure 2, the exact solution illustrated for this special case is obtained readily from Equation 21.

A simple technique with accuracy adequate for our purposes, suggested by Figure 2, is to calculate both limits, that is, Equations 21 and 23, then choose the smaller of the two.

For realistic cases, q is never as small as 0.1 (which implies $h \lesssim 1$ km) so the error near $q = 0$ is not significant. The maximum fractional error of about 30 percent occurs at $q = 2$, typically at the very high launch angle of 30°.

Much of the error is removed by a final adjustment which forces the r_i to precisely sum to the correct range.

4.2 Example

An example which stresses the algorithm somewhat is summarized in Table 1. The transmitter is located at Washington, D.C. and the receiver at Tel Aviv, at 84.92° great circle distance (9432 km). Ionospheric conditions are appropriate for 0600 UT, which places the western two-thirds of the link in darkness (local time in Washington is about 1:00 a.m. and in Tel Aviv is about 8:30 a.m.)

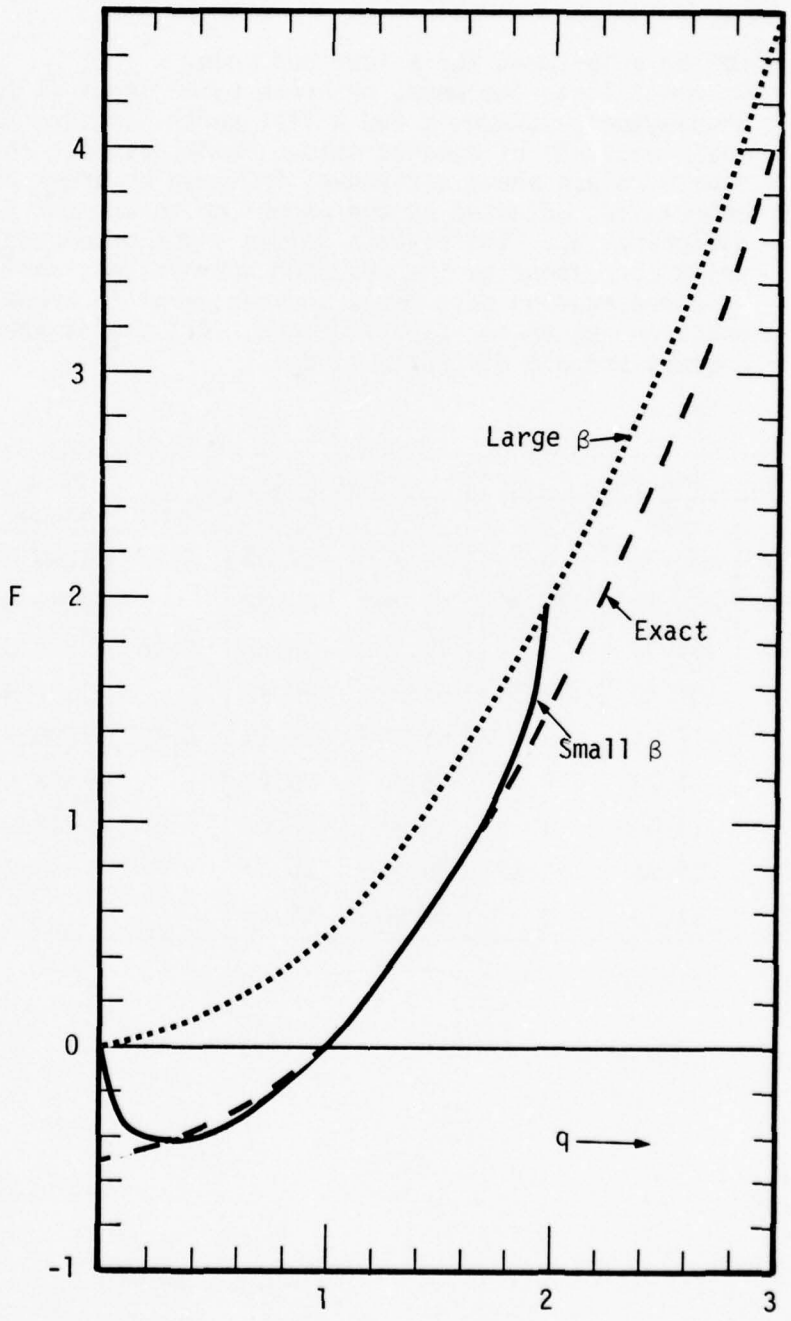

Figure 2. Reflection height adjustment. Small and large β limiting solutions to (19) are compared to the exact solution for a special case.

Table 1. Height adjustment for a four-hop mode. Column 1 lists the pass, or break point index (1 is Washington), columns 2 and 3 list north latitude and east longitude of equally spaced break points. The fourth column shows altitudes, followed by break point coordinates adjusted by the algorithm to account for differing h_r. The seventh column lists ground angles which correspond to the adjusted coordinates, followed by corresponding pass range and the error in break point position due to our approximation. All angles are in degrees and all distances in km.

Break Point	Equal Spacing			Adjusted for h_r			Pass Range	Position Error
	Lat.	Long.	h_r	Lat.	Long.	Angle		
1	38.90	-77.03	0	38.90	-77.03	6.97	1260.81	0
2	44.84	-65.19	290.30	45.20	-64.28		1260.81	1.88
3	49.30	-51.01	0	49.77	-48.86	6.96	1310.66	3.76
4	51.74	-34.72	307.53	51.98	-30.43		1310.66	6.43
5	51.75	-17.54	0	51.15	-11.44	6.92	1598.57	9.10
6	49.35	-1.23	417.43	46.34	9.22		1598.57	6.59
7	44.91	13.00	0	38.51	25.65	7.05	548.21	4.08
8	38.99	24.86	92.67	35.37	30.39		548.21	2.04
9	32.06	34.76	0	32.06	34.76			0

The mode illustrated has 4-hops, three F2-layer reflections and one E-layer reflection. As the ray traverses the great circle path successive reflections occur at increasing effective altitudes until the last reflection, which is at sharply decreased altitude. The reasons for this behavior illustrate the complicated interplay of ionospheric behavior and radio propagation. The second reflection point is above the first predominantly because the F2 and F1 layers are weaker at the second hop (break point 4 in Table 1) where the local time is about 4:15 a.m. The third hop (break point 6) has higher effective altitude despite the dawn buildup of the F2 layer, because the F1 layer is nearly strong enough to reflect the ray and thus refracts strongly. Finally at the fourth hop (break point 8) not only is the F1 layer capable of reflecting the ray but also the E-layer can reflect and our algorithm chooses the lower mode.

An exact solution would have yielded equal angles approximately 7.008°. Thus the seventh column of the table can be used as a measure of inaccuracy of our algorithm. Another measure, one which is more directly pertinent to nuclear effects, is the error in placement of the break points. This error measures the distance by which a disturbance, beta patch or other, might be missed and is shown in the final column. The error is seen to build up to about 9 km then fall back toward zero, despite the fact that break points were shifted as much as 1397 km (No. 7). Since any natural or nuclear disturbance of interest will be large compared to 9 km one concludes that the approximation is adequate.

5. AMBIENT IONOSPHERIC TILT ANGLE CALCULATION

The main motivation for inclusion of ambient ionospheric tilt effects is to establish a mechanism by which tilt effects in a highly disturbed ionosphere can be calculated. For this reason we neglect lower refracting layer effects and treat only reflecting layer tilt.

In the sketch the solid lines illustrate real ray paths, one of which connects points (1) and (2). This ray reaches a maximum height, h_m, and is to be represented by an equivalent triangular path which reflects at height h_r, illustrated by dotted lines. To find the effective tilt angle, τ, of the reflection point, we calculate the true maximum height, h_m', of a similar ray, with points (1) and (2) displaced a distance δr. Then

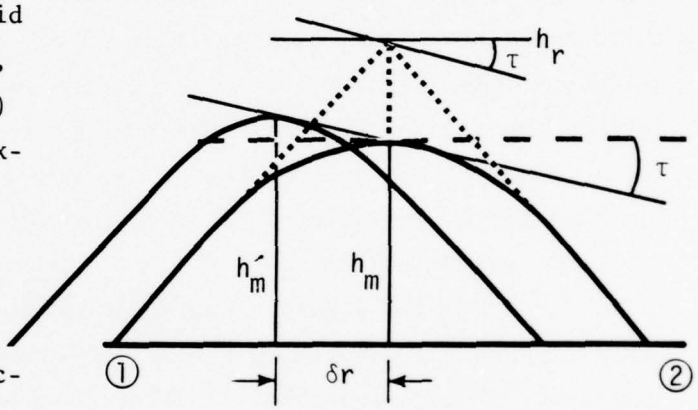

$$\tau = \frac{(h_m - h_m')}{\delta r} \tag{30}$$

Equation 30 is good to first order which is adequate for the first treatment of this effect; we do not hope for accuracy when τ is large. For the moment, and perhaps forever, it will have to be sufficient to know that the mode is highly disturbed when τ is large, and the approximate degree of disturbance.

5.1 Tilt Parallel to the Great Circle Path

After calculation of the first approximation to reflection, described in Section 3, the true maximum ray penetration height, h_m, is known from Equation 4 and the corresponding value of x from Equation 1. It only remains to choose one or more other points along the great circle path to calculate h_m', using the same value of x. Since the ionosphere is described by parameters specified at points along the great circle, the technique adopted is to locate the two great circle ionospheric data points surrounding the reflection point, evaluate h_m at these two points, then calculate "parallel tilt", $\tau_{\parallel}$ from (30). If the ray is capable of penetrating the ionosphere at one of the great circle data points, the reflection point is used in its place. The convention is adopted that tilt is positive if height increases toward the receiver.

5.2 Tilt Perpendicular to the Great Circle Path

It would seem that our method of ionospheric description, which restricts knowledge of ionospheric parameters to those along the great circle path, might prevent finding tilt angles perpendicular to the great great circle. This is not the case because at each point on the great circle path the ionospheric data table covers all 24 hours of local time. This is equivalent to data at all values of longitude provided effects of geomagnetic coordinate changes on the longitude dependence in the neighborhood of the point of interest are neglected.

The situation is depicted in the sketch. We know the latitude, longitude coordinate of the reflection point (λ,ℓ), and the two great circle ionospheric data points surrounding it (λ_1,ℓ_1) and (λ_2,ℓ_2). The tilt angle

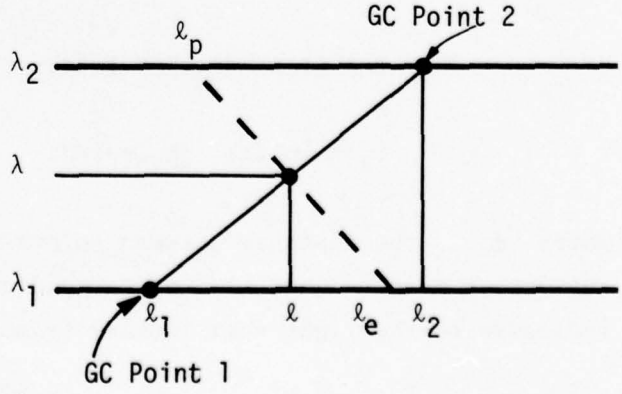

perpendicular to the great circle path can be obtained by differencing h_m at the points (λ_1,ℓ_e) and (λ_2,ℓ_p).

Since arc lengths between great circle data points are small, plane geometry will suffice. In this approximation the interesting longitudes are given by

$$\ell_e = \ell + (\lambda-\lambda_1)(\lambda_2-\lambda_1)/(\ell_2-\ell_1) \tag{31}$$

$$\ell_p = \ell + (\lambda-\lambda_2)(\lambda_2-\lambda_1)/(\ell_2-\ell_1) \tag{32}$$

If the local time at (λ,ℓ) is t, then ionospheric parameters for (λ_1,ℓ_e) can be obtained by evaluating those at (λ_1,ℓ_1) at

$$t_e = t + \alpha(\ell_e-\ell) \tag{33}$$

where α is the factor appropriate to convert longitude to time (in our case ionospheric time is measured in radians from local midnight, so $\alpha = 1$). Similarly

$$t_p = t + \alpha(\ell_p-\ell) \tag{34}$$

is the local time appropriate for point (λ_2,ℓ_p).

Then the perpendicular tilt, $\tau_\perp$, is obtained from

$$\tau_\perp = [h_m(e) - h_m(p)]/d \tag{35}$$

where d is the distance between points (λ_1,ℓ_e) and (λ_2,ℓ_p). Note the convention adopted here is that perpendicular tilt is positive if height increases to the right when looking from transmitter toward receiver.

There are two special cases. If the path segment $1 \rightarrow 2$ is very nearly North-South ($|\ell_2 - \ell_1| < 10^{-2}$ rad) we evaluate h_m at (λ, ℓ + 20 minutes) and (λ, ℓ - 20 minutes). If the path segment $1 \rightarrow 2$ lies too nearly East-West ($|\lambda_2 - \lambda_1| < 10^{-2}$ rad) this scheme fails and zero perpendicular tilt is assumed.

6. EFFECT OF IONOSPHERIC TILT ALONG THE GREAT CIRCLE PATH

Consider the case of a propagating mode with arbitrary but fixed number of hops where the ionosphere varies along the path such that each hop has a different virtual reflection height, h_i, and has a small tilt angle, τ_i; but the ray remains in the great circle. As before, the path is composed of straight line segments which are called "passes" connected at "break points". Thus an n-hop mode consists of 2n passes and 2n + 1 break points as depicted in the sketch below, for a 4-hop mode.

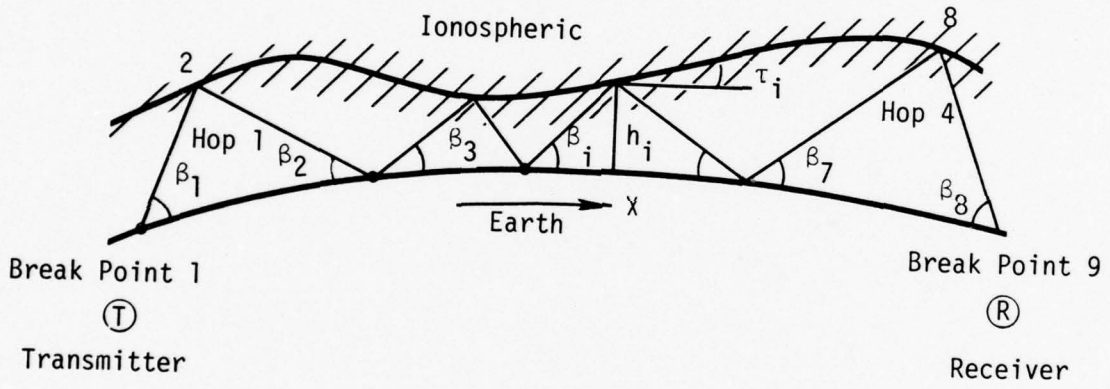

Break Point 1

Ⓣ

Transmitter

Break Point 9

Ⓡ

Receiver

The tilt angles are given by

$$\tau_i = \left.\frac{dh}{dx}\right|_i \quad . \tag{36}$$

The entire mode geometry has been calculated as previously described including effects of varying reflection height, but under the assumption that the ionosphere is circularly symmetric about the center of the earth at each reflection point, that is, effects of tilt have been neglected. A formalism is needed to modify break point coordinates to account for tilt, one which is accurate for reasonably small deflections and "sensible" for large. By "sensible" we mean the break point range should be monotone increasing with break point, reflection altitude shouldn't suffer a major fractional change, etc.

6.1 Single Hop - Plane Geometry

Initially consider the problem of a single hop in plane geometry, then one can work toward a multihop problem in circular geometry. In the sketch below, dashed lines show the situation which would obtain if the ionosphere were parallel to the surface of the earth while solid lines show the situation which obtains when the ionosphere has a (positive) tilt angle τ.

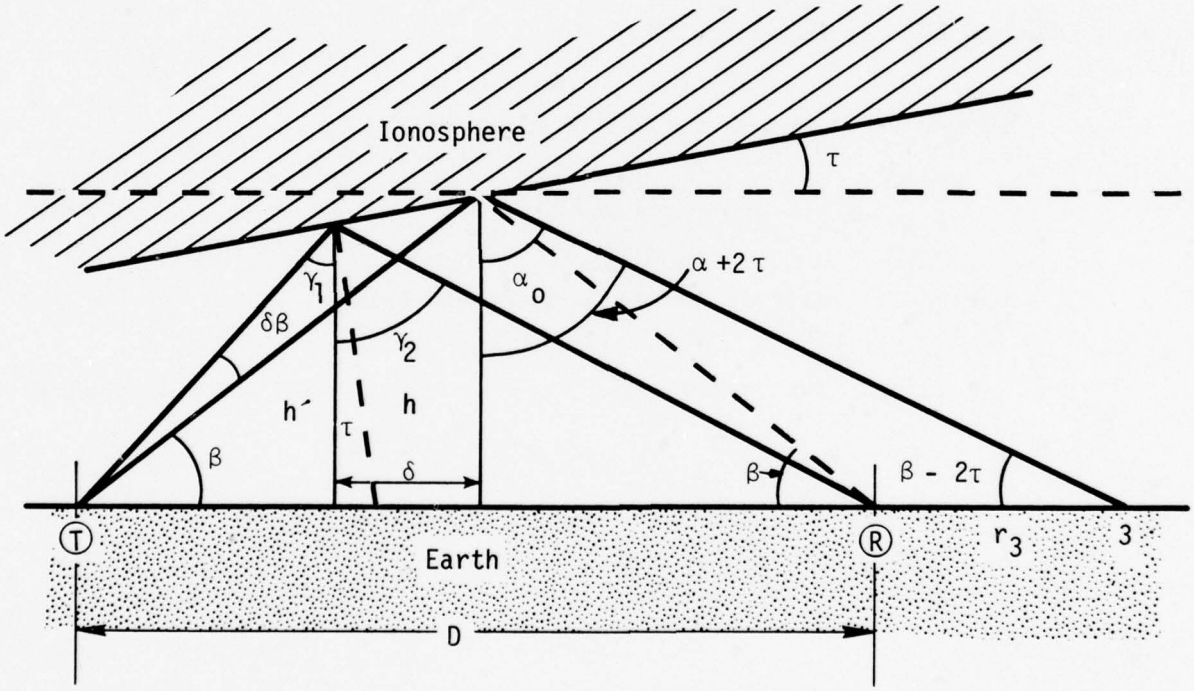

From the sketch, the launch angle without tilt is

$$\text{ctn}\,\beta = \tan\,\alpha_o = \frac{D}{2h} \tag{37}$$

and, if launched at angle β , the ray will be land beyond the receiver at angle $\beta-2\tau$.

$$\text{ctn}\ (\beta-2\tau) = \frac{D}{2h} + \frac{r_3}{h} \tag{38}$$

As a first step in finding the adjustment in β, h', and r required to force the ray to reach the receiver, search for an expression for the angle

$$\alpha = (\gamma_1 + \gamma_2)/2 \tag{39}$$

as a function of tilt angle τ.

Bisection of γ by the dashed line shows

$$\gamma_1 = \alpha - \tau \text{ and } \gamma_2 = \alpha + \tau \quad . \tag{40}$$

One useful relation can be found by combining

$$h'\tan\ (\alpha-\tau) = D/2 - \delta \tag{41}$$

and

$$h'\tan\ (\alpha-\tau) = D/2 + \delta \tag{42}$$

as

$$h'[\tan\ (\alpha+\tau) + \tan\ (\alpha-\tau)] = D \quad . \tag{43}$$

In order to eliminate h' another relation is required. Use

$$\tan\tau = (h-h')/\delta \tag{44}$$

with (41) to eliminate δ,

$$(h-h') \operatorname{ctn}\tau = \frac{D}{2} - h' \tan(\alpha-\tau) \tag{45}$$

Elimination of h' between (45) and (43) followed by an unusually tedious amount of trigonometric manipulation leads to the startling result

$$h \tan\alpha = D/2 \quad ! \tag{46}$$

In short, the angle by which the successful ray is reflected by the tilted ionosphere is equal to the untilted value, independent of τ. At risk of belaboring the obvious we point out that this result is not a small angle approximation but is exact.

Having established that the tilted and untilted cases have a common apex angle it is a short exercise in plane geometry to show that the launch angle has been raised

$$\delta\beta_T = \tau \tag{47}$$

while the receiving angle has been decreased by τ.

From (43), now that α is known to be constant, find the change in reflection altitude,

$$h' - h = \frac{2h \tan\alpha_o}{\tan(\alpha_o+\tau) + \tan(\alpha_o-\tau)} - h \quad . \tag{48}$$

After more exercise in trigonometric substitution, Equation 48 simplifies to

$$h' - h = - h \left(\frac{\sin\tau}{\sin\beta}\right)^2 \quad . \tag{49}$$

Using (44) one finds the ground range of the reflection point to have been shifted by an amount

$$\delta = \frac{h-h'}{\tan\tau} = -\, h\, \frac{\sin\tau\, \cos\tau}{\sin^2\beta} \quad , \tag{50}$$

where the minus sign is adopted to show that positive τ (reflection altitude increasing with ground range) produces a shift toward the transmitter.

This single hop case will be useful primarily as a check on approximate methods to be developed for more complex cases. Attempts at precision for more complex cases rapidly become bogged down in more trigonometry than justified on the basis of our assumption of constant τ in the vicinity of a given break point.

6.2 Heights Constant - One Place Tilted - Plane Geometry

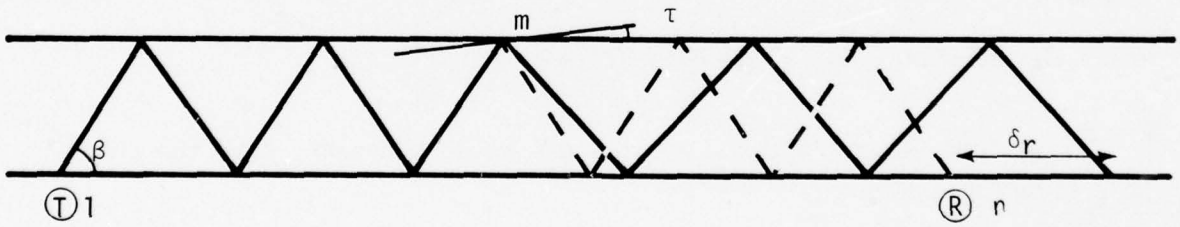

Now consider the cumulative effects of multiple hops on break point range. In the sketch a ray has been launched at angle β appropriate for a multiple hop path to the receiver at Ⓡ , the n^{th} break point.

The tilt τ causes reflection angles to change by 2τ after point m. Thus the distance, δr, by which the receiver is missed is

$$\delta r = (n-m)\, h(\mathrm{ctn}(\beta-2\tau) - \mathrm{ctn}\beta)$$

$$\approx (n-m)\, h(1+\mathrm{ctn}^2\beta)2\tau \quad . \tag{51}$$

The total range from Ⓣ to Ⓡ is

$$R = (n-1)\, h\, \mathrm{ctn}\beta \quad . \tag{52}$$

then

$$\frac{dR}{d\beta} = -\,(n-1)h(1+\mathrm{ctn}^2\beta) \quad . \tag{53}$$

So the change in launch angle required to bring the ray down on the receiver is found from requiring

$$\frac{dR}{d\beta}\,\delta\beta = -\,\delta r$$

and is

$$d\beta = 2\,\frac{(n-m)}{(n-1)}\,\tau \quad . \tag{54}$$

We can check our approximation by noting that for a one-hop case, $n = 3$, $m = 2$, (54) gives

$d\beta = \tau$, the exact answer, while for an extreme case, m small, $n \to \infty$

$$d\beta \to 2\tau,$$

Reference to the sketch shows the angle 2τ to be the one which yields the unperturbed angle β thereafter. For this extreme case the approximation has introduced an error equivalent to the miss distance on one hop, an error commensurate with current understanding of the ionosphere, especially so because some of the error can be eliminated by retroactive adjustment of break points to force the ray to land on the receiver.

The increment in range at intermediate break points is given by

$$\delta r_i = \begin{cases} h \operatorname{ctn} \left[\beta + 2 \frac{(n-m)}{(n-1)} \tau\right] , & i \leq m \\ h \operatorname{ctn} \left[\beta - 2 \frac{(m-1)}{(n-1)} \tau\right] , & i > m \end{cases} \qquad (55)$$

6.3 Heights Vary - One Place Tilted - Plane Geometry

To find the miss distance we must sum heights in Equation 51

$$\delta r_n = \sum_{m}^{n} h_i (1+\operatorname{ctn}^2\beta)\, 2\tau$$

$$= 2\,(1+\operatorname{ctn}^2\beta)\tau \sum_{m+1}^{n} \left|h_i - h_{i-1}\right| \quad . \qquad (56)$$

Following an argument similar to the previous case we find

$$\delta\beta = \tau \frac{2 \sum_{m+1}^{n} \left|h_i - h_{i-1}\right|}{\sum_{2}^{n} \left|h_i - h_{i-1}\right|} \quad . \qquad (57)$$

6.4 Heights Vary - All Places Tilted - Plane Geometry

From (57) the change in launch angle due to tilt at location m is

$$\delta\beta_m = \tau_m \frac{2\sum_{i=m+1}^{n} h_i}{\sum_{i=2}^{n} h_i} \tag{58}$$

The total change in launch angle is given by summing (58);

$$\delta\beta = \frac{2\sum_{m=2}^{n-1} \tau_m \sum_{i=m+1}^{n} h_i}{\sum_{m=2}^{n} h_i} \quad . \tag{59}$$

The simplest method of finding the new ranges and heights of break points is to accumulate them, viz.

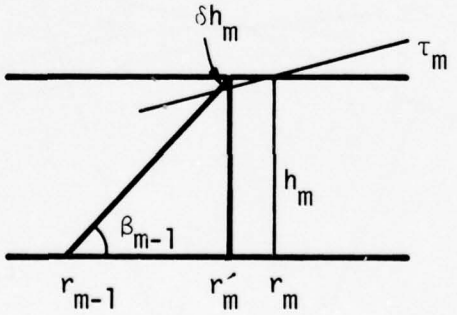

$$\beta_{m-1} = \beta_{m-2} - 2\tau_{m-1} \quad ,$$

$$r'_m = r_{m-1} + h_m \operatorname{ctn}\beta_{m-1} \quad , \tag{60}$$

and

$$\delta h_m = (r_m' - r_m)\tan \tau_m \tag{61}$$

where a second order effect in the equation for r_m has been neglected.

When one reaches the last break point the accumulated error is measured by the miss distance. All ranges are then scaled to force agreement in total range.

6.5 Extension to Circular Geometry

If β is interpreted as the launch angle relative to the chord of the arc as depicted below nothing changes to first order in the pass range over the radius of the earth.

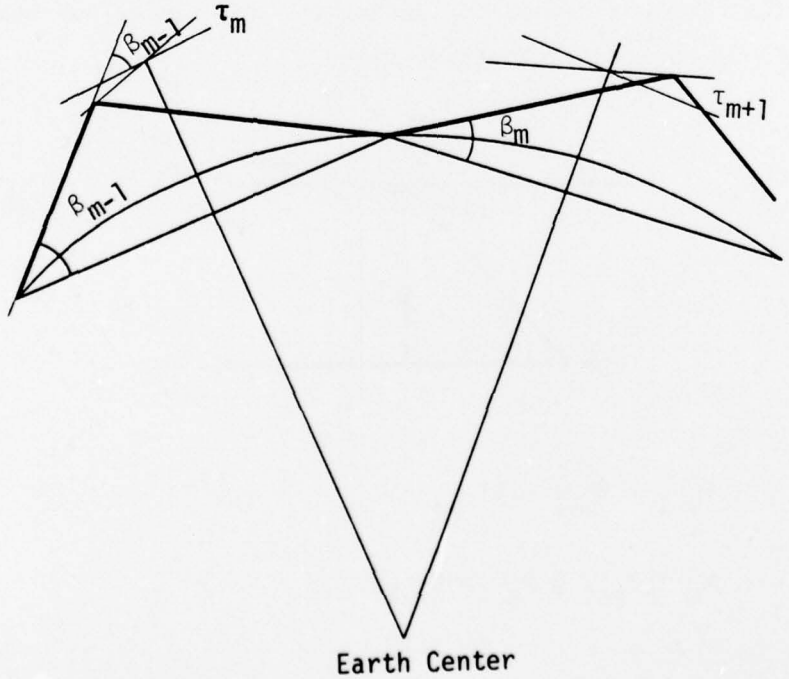

It is necessary, however, to rederive (59) accounting for the fact that, while incident and reflection angles are equal relative to the earth's surface, they are not equal relative to the chord of the arc. The effect of this extension is that the factor $(1+\text{ctn}^2\beta)$ cannot be regarded as constant, but must be retained. Equation 59 becomes

$$\delta\beta = \frac{2\sum_{m=2}^{n-1}\tau_m \sum_{i=m+1}^{n} h_i(1+\text{ctn}^2\beta_i)}{\sum_{i=2}^{n} h_i(1+\text{ctn}^2\beta_i)} \qquad (62)$$

In many cases a second order term due to the change in incident angle which results from change in pass range is significant. Proper treatment of this term is a bit cumbersome and more importantly, tends to destabilize the adopted mathematical treatment. A satisfactory expedient is to retroactively adjust all pass ranges, to force agreement with total range, by an amount proportional to the square of the calculated pass range.

6.6 Example

Table 2 summarizes results of the approximate treatment developed above when applied to the same four-hop Washington to Tel Aviv mode illustrated previously. This particular mode was chosen primarily because it represents as difficult a case for the parallel tilt approximation as has been encountered to date. The table shows errors as large as about 20 km in placement of break points. Since this error is small compared to the size of any possible D-layer absorbing region the method is considered satisfatory. The calculated launch angle at Washington is 5.11° compared to the exact solution of 5.01° and the calculated received angle at Tel Aviv is 12.15° compared to the exact solution of 11.89°.

Table 2. Parallel tilt adjustment for a 4-hop mode. Column 1 lists the break point index (1 is Washington, D.C., 9 is Tel Aviv). The next three columns list latitude, longitude, and great circle range measured from Washington after adjustment for different reflection height. The following four columns show the tilt angle parallel to the great circle path, reflection height and position adjustments for tilt and the increase in range due to tilt. The next column shows the exact trigometric position (accepting h_r) and the last column the amount by which the approximate method overestimates the position. All distances are in km and all angles in degrees.

Break Point	h_r Adjusted			Adjusted for Tilt				"Exact" Position	Position Error
	Lat.	Long.	Position	Tilt	h_r	Position	Change		
1	38.90	-77.03	0	0		0	0	0	0
2	45.20	-64.28	1260	-0.18	290.03	1400	140	1408	-8
3	49.77	-48.86	2521	0	0	2715	194	2724	-19
4	51.98	-30.43	3831	0.27	308.50	4087	256	4094	-7
5	51.15	-11.44	5141	0	0	5601	460	5620	-19
6	46.34	9.22	6739	-1.34	408.41	7408	669	7418	-10
7	38.51	25.65	8337	0	0	8684	347	8672	12
8	35.37	30.39	8885	-0.04	92.54	9059	174	9054	5
9	32.06	34.76	9433	0	0	9433	0	9433	0

7. TILT ACROSS GREAT CIRCLE

7.1 Plane Case

Looking from transmitter toward receiver, one sees a tilted ionosphere and the ray path. Positive tilt means h increases to the right as depicted below. Launch a ray along the great circle path. Without tilt one would see only one vertical line. With tilt η_m at break point m the ray is deflected to the right.

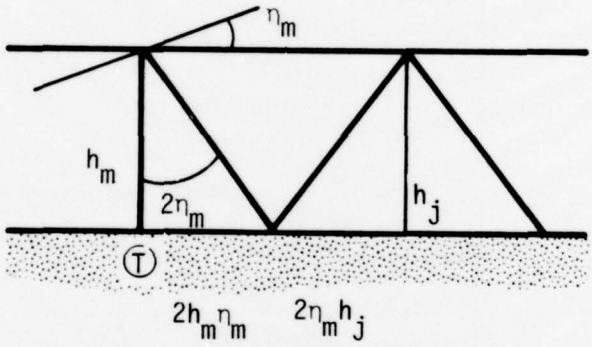

The ray comes off the ionosphere at angle $2\eta_m$, causing it to land a distance $2h_m\,\eta_m$ to the right of the great circle path, then if there are no more tilted break points, it moves additional distance $2\eta_m h_j$ for each pass.

The total displacement at the end of the path, break point n, due to the tilt at break point m is

$$d_m = 2\eta_m \sum_{i=m+1}^{n} \left| h_i - h_{i-1} \right| \quad . \tag{63}$$

If one assumes a tilt at each break point, one has

$$d = \sum_{m=2}^{n-1} d_m = 2 \sum_{m=2}^{n-1} \eta_m \sum_{i=m+1}^{n} \left| h_i - h_{i-1} \right| \quad . \tag{64}$$

The launch azimuth (positive to right) of the ray which reaches the receiver must counteract the deflection;

$$\alpha_L = - d/R \tag{65}$$

where R is the great circle range of the total path.

The azimuth of the ray at the receiver is

$$\alpha_R = - d_{n-1}/r_n \tag{66}$$

where r_n is the ground range of the final pass.

Since the launch azimuth is α_L, the resulting displacement perpendicular to the great circle of the J^{th} break point is

$$S_J = 2 \sum_{m=2}^{J-1} \eta_m \sum_{i=m+1}^{J} \left| h_i - h_{i-1} \right| + \alpha_L d_J \tag{67}$$

where d_J is ground range to point J.

The new reflection altitude is

$$h_J' = h_J + S_J \tan \eta_J \quad . \tag{68}$$

Numerically it is convenient to collect $\sum_{i=m+1}^{n} \left| h_i - h_{i-1} \right|$ and $\sum_{m=2}^{J-1} \eta_m$, then

$$S_J = S_{J-1} + 2\eta_{J-1} \sum_{i=J}^{J} \left| h_i - h_{i-1} \right| + 2 \left| h_J - h_{J-1} \right| \sum_{m=2}^{J-1} \eta_m + \alpha_L r_J$$

$$= S_{J-1} + 2\eta_{J-1} \left(\sum_{i=2}^{n} \left| h_i - h_{i-1} \right| - \sum_{i=J+1}^{n} \left| h_i - h_{i-1} \right| \right) + 2 \left| h_J - h_{J-1} \right| \sum_{m=2}^{J-1} \eta_m + \alpha_L r_J \tag{69}$$

where r_J is the incremental range of the J^{th} pass.

7.2 Extension to Spherical Geometry

If h_i is interpreted as the height of reflection above the chord of the hop rather than above the earth's surface, Equation 69 is still valid.

7.3 Determination of Break Point Horizontal Coordinates

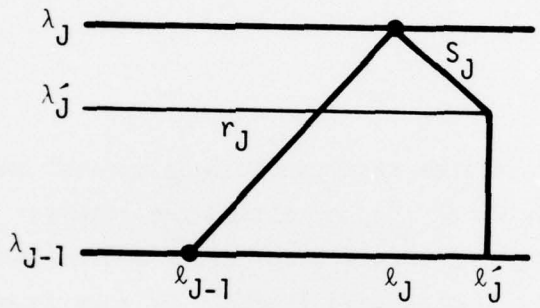

If λ is colatitude and ℓ is longitude, to a good approximation one can write

$$S_J = R_e \sqrt{(\delta\lambda)^2 + \sin^2 \lambda_J \, (\delta\ell)^2} \tag{70}$$

Since the slope of the line segment S_J is the negative gradient of the line segment r_J,

$$\left.\frac{d\lambda}{d\ell}\right|_s = - \left(\frac{d\lambda}{d\ell}\right)_r^{-1} = - \frac{(\ell_J - \ell_{J-1})}{(\lambda_J - \lambda_{J-1})} \quad , \tag{71}$$

combining (70) and (71),

$$\delta\lambda = \frac{\pm S_J}{R_e \sqrt{1 + \sin^2 \lambda_J (\lambda_J - \lambda_{J-1})^2 / (\ell_J - \ell_{J-1})^2}} \quad , \tag{72}$$

where the positive sign is chosen if $\ell_J > \ell_{J-1}$, and,

$$\delta\ell_J = \frac{\pm S_J}{R_e\sqrt{(\ell_J-\ell_{J-1})^2/(\lambda_J-\lambda_{J-1})^2 + \sin^2\lambda_J}} \tag{73}$$

where the positive sign is chosen if $\lambda_J < \lambda_{J-1}$.

7.4 Example

Table 3 illustrates results obtained for the Washington-Tel Aviv case. The distance by which the ray missed the receiver (1.5 parts in 10^5) measures the combination of second order error in the technique and round off error in a 32 bit computer word length. Of more interest is the much lower magnitude of perpendicular displacements relative to parallel displacements. Most of this reduction in effect is due to the circumstance that the path lies mostly East-West so that perpendicular gradients are smaller than parallel gradients and the further accident that perpendicular tilts tend to cancel (the first two angles sum to +0.26 and the next is -0.26). However, parallel gradients systematically tend to be about an order of magnitude more effective in displacement than perpendicular gradients. The parallel effect tends to be enhanced by small angle of incidence at the earth, while the perpendicular effect always acts as though the ray were near a right incident angle.

Table 3. Perpendicular tilt adjustment for a 4-hop Mode. Column 1 lists the mode break point index, column 2 reflection altitude, and column 3 the tilt angle perpendicular to the great circle path. Column 4 lists displacement of break point, positive to right of great circle path as viewed from the transmitter, and column 5 the adjusted reflection height due to perpendicular tilt. All distances are in kilometers and all angles in degrees.

Break Point	h_r	η	After Adjustment	
			S	h
1	0	0	0	0
2	290.03	0.11	-1.29	290.03
3	0	0	-1.40	0
4	308.50	0.15	-1.49	308.49
5	0	0	0.02	0
6	408.41	-0.26	2.34	408.40
7	0	0	0.91	0
8	92.54	-0.03	0.43	92.54
9	0	0	-0.14	0

REFERENCES

1. Knapp, W., General Electric-TEMPO, private communication.

2. Sowle, D. H., private communication.

3. Hayden, Leften, and Rosich, Predicting the Performance of High Frequency Sky-Wave Communication Systems (The Use of HFMUFES 4 Program), U.S. Dept. of Commerce, Office of Telecommunication, OT Report 76-102, Sept. 1976.

4. Bauman, E., and W. Jaye, Stanford Research Institute, private communication.

5. Barghausen, Finney, Procter, and Schultz, Predicting Long-Term Operational Parameters of HF Sky-Wave Telecommunication Systems, ESSA Report, ERL-110-ITS78.

6. Feniger and Gambill, A Fortran Code for Computation of Weapon Radiation Effects on Communication Systems, Vol. 1, User's Guide, General Electric-TEMPO, GE73TMP-15, Aug. 1973.

7. Ching and Chiu, "A Phenomological Model of Global Ionospheric Electron Density in the E-, F1-, and F2-Regions," J. Atm. and Terr. Phys., 35, pp 1615-1630, 1973.

DISTRIBUTION LIST

DEPARTMENT OF DEFENSE

Assistant Secretary of Defense
Cmd, Cont. Comm. & Intell.
ATTN: M. Epstein
ATTN: J. Babcock

Director
Command Control Technical Center
ATTN: C-650, W. Heidig
ATTN: C-650, G. C. Jones
ATTN: C-312, R. Mason

Director
Defense Advanced Rsch. Proj. Agency
ATTN: Nuclear Monitoring Research
ATTN: Strategic Tech. Office

Defense Communication Engineer Center
ATTN: Code R410, James W. McLean
ATTN: Code R820, R. L. Crawford
ATTN: Code R220, M. Horowitz
ATTN: Code 720, John Worthington

Director
Defense Communications Agency
ATTN: Code 810, R. W. Rostron
ATTN: Code 101B, Maj Rood
ATTN: Code 480
ATTN: Maurey Raffensperger

Defense Communications Agency
WWMCCS System Engineering Org.
ATTN: R. L. Crawford

Defense Documentation Center
Cameron Station
12 cy ATTN: TC

Director
Defense Intelligence Agency
ATTN: W. Wittig, DC-7D
ATTN: DT-1B
ATTN: DIAST-5
ATTN: DIAAP, Albert L. Wise
ATTN: DT-1BZ, Capt R. W. Morton
ATTN: HQ-TR, J. H. Stewart
ATTN: DB-4C, Edward O'Farrell

Director
Defense Nuclear Agency
ATTN: DDST
ATTN: STVL
ATTN: TISI Archives
3 cy ATTN: RAAE
3 cy ATTN: TITL, Tech. Lib.

Commander, Field Command
Defense Nuclear Agency
ATTN: FCPR

Director
Interservice Nuclear Weapons School
ATTN: Document Control

DEPARTMENT OF DEFENSE (Continued)

Director
Joint Strat. Tgt. Planning Staff, JCS
ATTN: JPST, Capt G. D. Goetz
ATTN: JLTW-2

Chief
Livermore Division, Field Command, DNA
Lawrence Livermore Laboratory
ATTN: FCPRL

Director
National Security Agency
ATTN: Frank Leonard
ATTN: John Skillman, R52
ATTN: Pat Clark, W14
ATTN: Oliver H. Bartlett, W32

OJCS/J-3
ATTN: WWMCCS Eval. Ofc., Mr. Toma

Under Secretary of Def. for Rsch. & Engrg.
ATTN: S&SS (OS)

DEPARTMENT OF THE ARMY

Commander/Director
Atmospheric Sciences Laboratory
U.S. Army Electronics Command
ATTN: DELAS-AE-M, F. E. Niles

Chief C-E Services Division
U.S. Army Communications Cmd.
ATTN: CC-OPS-CE

Commander
Harry Diamond Laboratories
ATTN: DELHD-RB, Robert Williams
ATTN: DELHD-NP, Francis N. Wimenitz
ATTN: DRXDO-NP, Cyrus Moazed
ATTN: DRXDO-TI, Mildred H. Weiner

Director
TRASANA
ATTN: ATAA-TAC, LTC John Hesse
ATTN: TCC, F. Payan, Jr.
ATTN: ATAA-SA

Commander
U.S. Army Comm-Elec. Engrg. Instal. Agy.
ATTN: EED-PED, George Lane
ATTN: EED-PED, Ward Nair

Commander
U.S. Army Electronics Command
ATTN: DRSEL-PL-ENV, Hans A. Bomke
ATTN: J. E. Quigley

Commander
U.S. Army Foreign Science & Tech. Ctr.
ATTN: R. Jones
ATTN: P. A. Crowley

DEPARTMENT OF THE ARMY (Continued)

Commander
U.S. Army Materiel Dev. & Readiness Cmd.
ATTN: DRCLDC, J. A. Bender

Commander
U.S. Army Missile Command
ATTN: DRSMI-YTT, W. G. Preussel, Jr.

Commander
U.S. Army Nuclear Agency
ATTN: MONA-WE, J. Berberet

Director
U.S. Army Ballistic Research Labs.
ATTN: Tech. Lib., Edward Baicy

Commander
U.S. Army Satcom Agency
ATTN: Document Control

DEPARTMENT OF THE NAVY

Chief of Naval Operations
ATTN: Op-943, LCDR Huff

Chief of Naval Research
ATTN: Code 461
ATTN: Code 402
ATTN: Code 420
ATTN: Code 421

Commander
Naval Electronic Systems Command
Naval Electronic Systems Cmd. Hqs.
ATTN: PME 117
ATTN: NAVALEX 034, T. Barry Hughes
ATTN: PME 117-T, Satellite Comm. Proj. Off.

Commanding Officer
Naval Intelligence Support Ctr.
ATTN: Mr. Dubbin, STIC 12
ATTN: J. Galet, Code 5404

Commander
Naval Ocean Systems Center
3 cy ATTN: Code 2200
ATTN: Code 0230, C. Baggett
ATTN: R. Eastman
ATTN: Code 532, William F. Moler

Director
Naval Research Laboratory
ATTN: Code 5400, Hg. Comm. Dir., Bruce Wald
ATTN: Code 5460, Electromag Prop. Br.
ATTN: Code 5465, Prop. Applications
ATTN: Code 5430, Satellite Comm.
ATTN: Code 7701, Jack D. Brown
ATTN: Code 7700, Timothy P. Coffey
ATTN: Code 5410, John Davis

Commander
Naval Space Surveillance System
ATTN: CAPT J. H. Burton

Naval Space System Activity
ATTN: A. B. Hazzard

DEPARTMENT OF THE NAVY (Continued)

Officer-in-Charge
Naval Surface Weapons Center
ATTN: Code WA 501, Navy Nuc. Prgms. Off.

Commander
Naval Surface Weapons Center
Dahlgren Laboratory
ATTN: R. F. Butler, DF-14

Officer-in-Charge
Naval Underwater Systems Center
New London Laboratory
ATTN: Peter Bannister

Director
Strategic Systems Project Office
ATTN: NSSP-2722, Fred Wimberly
ATTN: NSP-2141

DEPARTMENT OF THE AIR FORCE

Commander
ADC/DC
ATTN: DC, Mr. Long

Commander
ADCOM/XPD
ATTN: XPQDQ
ATTN: XP

AF Geophysics Laboratory, AFSC
ATTN: LKB, Kenneth S. W. Champion
ATTN: OPR, James C. Ulwick
ATTN: OPR, Alva T. Stair
ATTN: SUOL, Rsch. Lib.
ATTN: PHP, Jules Aarons
ATTN: PHD, Jurgen Buchau
ATTN: PHD, John P. Mullen

AF Weapons Laboratory, AFSC
ATTN: SUL
ATTN: SAS, John M. Kamm
ATTN: DYC, Capt L. Wittwer

AFTAC
ATTN: TF, Maj Wiley
ATTN: TN

Air Force Avionics Laboratory, AFSC
ATTN: AAB, H. M. Hartman
ATTN: AAD, Wade Hunt
ATTN: AAD, Allen Johnson

Headquarters
Electronics Systems Division/XR
ATTN: XRC, Lt Col J. Morin
ATTN: XRE, Lt Michaels

Headquarters
Electronic Systems Division/YS
ATTN: YSEV

Headquarters
Electronic Systems Division (AFSC)
ATTN: Jim Deas
ATTN: James Whelan

DEPARTMENT OF THE AIR FORCE (Continued)

Commander
Foreign Technology Division, AFSC
ATTN: ETD, B. L. Ballard
ATTN: NICD, Library

Hq. USAF/RD
ATTN: RDQ

Commander
Rome Air Development Center, AFSC
ATTN: EMTLD, Doc. Library
ATTN: V. Coyne, OCSE

Commander
Rome Air Development Center, AFSC
ATTN: ETEI, A. Lorentzen

SAMSO/MN
ATTN: MNNL, Lt Col Kennedy

SAMSO/SK
ATTN: SKA, Lt Maria A. Clavin

SAMSO/SZ
ATTN: SZJ, Maj Lawrence Doan
ATTN: SZ

SAMSO/YA
ATTN: YAT, Capt L. Blackwelder

Commander in Chief
Strategic Air Command
ATTN: XPFS, Maj Brian G. Stephan
ATTN: NRT
ATTN: ADWATE, Capt Bruce Bauer
ATTN: Chief Scientist

DEPARTMENT OF ENERGY

University of California
Lawrence Livermore Laboratory
ATTN: Tech. Info. Dept. L-3
ATTN: Frederick D. Seward, L-46
ATTN: Glenn C. Werth, L-216

Los Alamos Scientific Laboratory
ATTN: Doc. Con. for R. F. Taschek
ATTN: Doc. Con. for Donald R. Westervelt
ATTN: Doc. Con. for P. W. Keaton

Sandia Laboratories
ATTN: Doc. Con. for W. D. Brown, Org. 1353
ATTN: Doc. Con. for A. Dean Thornbrough, Org. 1245
ATTN: Doc. Con. for D. A. Dahlgren, org. 1722
ATTN: Doc. Con. for J. P. Martin, Org. 1732
ATTN: Doc. Con. for Space Proj. Div.
ATTN: Doc. Con. for 3141, Sandia Rpt. Coll.

Department of Energy
Albuquerque Operations Office
ATTN: Doc. Con. for D. W. Sherwood

Department of Energy
Division of Headquarters Services
ATTN: Doc. Con. for Allen Labowitz

DEPARTMENT OF ENERGY (Continued)

Sandia Laboratories
Livermore Laboratory
ATTN: Doc. Con. for Thomas B. Cook
ATTN: Doc. Con. for Byron E. Murphey

OTHER GOVERNMENT AGENCIES

Department of Commerce
Office of Telecommunications
Institute for Telecom Science
ATTN: G. Reed
ATTN: L. A. Berry
ATTN: William F. Utlaut
ATTN: A. Glenn Jean
ATTN: D. D. Crombie

NASA
Goddard Space Flight Center
ATTN: ATS-6 Ofc., P. Corrigan

National Oceanic & Atmospheric Admin.
Environmental Research Laboratories
ATTN: C. L. Rufenach
ATTN: Joseph H. Pope
ATTN: Richard Grubb

Department of Commerce
National Bureau of Standards
ATTN: Raymond T. Moore

Department of Transportation
Office of the Secretary
ATTN: R. L. Lewis
ATTN: R. H. Doherty

DEPARTMENT OF DEFENSE CONTRACTORS

Aeronomy Corporation
ATTN: S. A. Bowhill

Aerospace Corporation
ATTN: S. P. Bower
ATTN: V. Josephson
ATTN: D. P. Olsen, 120 Rm. 2224E
ATTN: Irving M. Garfunkel
ATTN: Norman D. Stockwell
ATTN: F. E. Bond, A1 Rm. 5003
ATTN: F. A. Morse, A6 Rm. 2407
ATTN: T. M. Salmi
ATTN: J. E. Carter, 120 Rm. 2209
ATTN: SMFA for PWW

Analytical Systems Engineering Corp.
ATTN: Radio Sciences

The Boeing Company
ATTN: Glen Keister
ATTN: D. Murray
ATTN: J. F. Kenny
ATTN: Glenn A. Hall

Brown Engineering Company, Inc.
ATTN: Romeo A. Deliberis

University of California at San Diego
Marine Physical Lab. of the Scripps
Institute of Oceanography
ATTN: Henry G. Booker

DEPARTMENT OF DEFENSE CONTRACTORS (Continued)

Charles Stark Draper Laboratory, Inc.
ATTN: J. P. Gilmore, MS 63
ATTN: D. B. Cox

Computer Sciences Corporation
ATTN: H. Blank

COMSAT Laboratories
ATTN: R. R. Taur

Cornell University
Department of Electrical Engineering
ATTN: D. T. Farley, Jr.

ESL, Inc.
ATTN: James Marshall
ATTN: J. Roberts
ATTN: C. W. Prettie
ATTN: V. L. Mower

Ford Aerospace & Communications Corp.
ATTN: J. T. Mattingley, MS X22

General Electric Company
Space Division
Valley Forge Space Center
ATTN: M. H. Bortner, Space Sci. Lab.

General Electric Company
TEMPO-Center for Advanced Studies
ATTN: Tim Stephens
ATTN: Mack Stanton
ATTN: Warren S. Knapp
ATTN: B. Gambill
ATTN: DASIAC
ATTN: Don Chandler

General Electric Company
ATTN: F. A. Reibert

General Research Corporation
ATTN: John Ise, Jr.
ATTN: Joel Garbarino

Geophysical Institute
University of Alaska
ATTN: Neal Brown
ATTN: Technical Library
ATTN: T. N. Davis

GTE Sylvania, Inc.
ATTN: Marshal Cross

HSS, Inc.
ATTN: Donald Hansen

University of Illinois
Department of Electrical Engineering
ATTN: K. C. Yeh

Institute for Defense Analyses
ATTN: Joel Bengston
ATTN: J. M. Aein
ATTN; Ernest Bauer
ATTN: Hans Wolfhard

Intl. Tel. & Telegraph Corporation
ATTN: Tech. Library

DEPARTMENT OF DEFENSE CONTRACTORS (Continued)

JAYCOR
ATTN: S. R. Goldman

Johns Hopkins University
Applied Physics Laboratory
ATTN: Thomas Potemra
ATTN: John Dassoulas
ATTN: Document Librarian

Linkabit Corporation
ATTN: Irwin Jacobs

Lockheed Missiles & Space Co., Inc.
ATTN: Dept. 60-12
ATTN: D. R. Churchill

Lockheed Missiles & Space Co., Inc.
ATTN: Martin Walt, Dept. 52-10
ATTN: Richard G. Johnson, Dept. 52-12
ATTN: W. L. Imhof, Dept. 52-12

MIT Lincoln Laboratory
ATTN: James H. Pannell, L-246
ATTN: D. Clark
ATTN: Lib. A-082 for David M. Towle
ATTN: Mr. Walden, X113

McDonnell Douglas Corporation
ATTN: William Olson
ATTN: N. Harris
ATTN: J. Moule
ATTN: George Mroz

University of Lowell Rsch. Foundation
ATTN: Dr. Bibl

Mission Research Corporation
ATTN: Dave Sowle
ATTN: F. Fajen
ATTN: R. Bogusch
ATTN: R. Hendrick
ATTN: P. Fischer
ATTN: M. Scheibe
ATTN: Steven L. Gutsche
5 cy ATTN: Tech. Lib.

The Mitre Corporation
ATTN: Chief Scientist, W. Sen
ATTN: C. E. Callahan
ATTN: G. Harding
ATTN: John Moganstern

Pacific-Sierra Research Corp.
ATTN: E. C. Field, Jr.

Pennsylvania State University
Ionosphere Research Laboratory
ATTN: Ionospheric Research Labs.

Photometrics, Inc.
ATTN: Irving L. Kofsky

Physical Dynamics, Inc.
ATTN: E. J. Fremouw

Physical Dynamics, Inc.
ATTN: A. Thompson
ATTN: Joseph B. Workman

DEPARTMENT OF DEFENSE CONTRACTORS (Continued)

R&D Associates
ATTN: Bryan Gabbard
ATTN: Robert E. Lelevier
ATTN: William J. Karzas
ATTN: William B. Wright, Jr.
ATTN: Forrest Gilmore
ATTN: H. A. Ory
ATTN: R. P. Turco

The Rand Corporation
ATTN: Cullen Crain
ATTN: Ed Bedrozian

Raytheon Company
ATTN: Barbara Adams

Science Applications, Inc.
ATTN: Jack McDougall
ATTN: Lewis M. Linson
ATTN: D. Sachs
ATTN: Curtis A. Smith
ATTN: E. A. Straker
ATTN: Daniel A. Hamlin

Science Applications, Inc.
Huntsville Division
ATTN: Dale H. Divis

DEPARTMENT OF DEFENSE CONTRACTORS (Continued)

SRI International
ATTN: M. Baron
ATTN: L. L. Cobb
ATTN: Ray L. Leadabrand
ATTN: Walter G. Chesnut
ATTN: G. Smith
ATTN: Walter Jaye
ATTN: Alan Burns
ATTN: Donald Neilson
ATTN: David A. Johnson
ATTN: Charles L. Rino
ATTN: Gary Price
ATTN: George Carpenter
ATTN: James R. Peterson

System Development Corporation
ATTN: E. G. Meyer

TRI-COM, Inc.
ATTN: Darrel Murray

TRW Defense & Space Sys. Group
ATTN: R. K. Plebuch, R1-2078
ATTN: Saul Altschuler
ATTN: Diana Dee

VisiDyne, Inc.
ATTN: J. W. Carpenter
ATTN: Charles Humphrey